International Journal of Biological Macromolecules xxx (xxxx) 1–11

Contents lists available at ScienceDirect

International Journal of Biological Macromolecules

journal homepage: www.elsevier.com/locate/ijbiomac

Effect of cationization pretreatment on the properties of cationic *Eucalyptus* micro/nanofibrillated cellulose

Jorge F.S. Pedrosa [a,*], Maria G. Rasteiro [a], Carlos P. Neto [b], Paulo J.T. Ferreira [a]

[a] CIEPQPF, Department of Chemical Engineering, University of Coimbra, Pólo II – R. Silvio Lima, 3030-790 Coimbra, Portugal
[b] RAIZ - Forest and Paper Research Institute, Quinta de São Francisco - Apartado 15, 3801-501 Eixo, Portugal

ARTICLE INFO

Keywords:
Cationization
Fibrillated cellulose
Quaternary ammonium
Rheology

ABSTRACT

Micro/nanofibrillated celluloses (M/NFCs) have attracted considerable research interest over the past few decades, with various pretreatments being used to reduce energy consumption and/or increase fibrillation. To date, few studies have considered cationization as a pretreatment for their preparation. In this work, quaternary ammonium groups were attached to cellulose fibers by a direct reaction with 2,3-epoxypropyltrimethylammonium chloride or by a two-step method (periodate oxidation + Girard's reagent T). The cationic fibers with degrees of substitution (DS) between 0.02 and 0.36, were subjected to homogenization treatment.

The morphological properties, chemical composition, and rheological behavior were evaluated to assess the effect of DS and the effect of the cationization method (for samples with similar DS). The two-step cationization resulted in significant degradation of the cellulose structure, leading to the formation of short fibrils and solubilization of the material, ranging from 6% to almost complete solubilization at a DS of 0.36. Direct cationization resulted in longer fibrils with an average diameter of 1 μm, and no significant cellulose degradation was observed, leading to a more cohesive gel-like material (at 1 wt%). These observations clearly show the strong influence of the cationization method on the final properties of the cationic cellulosic materials.

1. Introduction

The petroleum-based economy that has driven the development of modern society over the last century is showing signs of decline. The depletion of natural resources requires humanity to be more alert about the sustainability of our planet, forcing a shift in mentality towards alternative renewable sources.

Cellulose, primarily derived from lignocellulosic sources in the form of fibers, is considered the most abundant renewable biopolymer in the world, with an estimated annual biosynthesis of about 10^{11} tons [1], it appears as a logical alternative raw material for the development of new biobased products.

Cellulose is recalcitrant to dissolution in most common solvents [2]. For this reason, the deconstruction of cellulose fibers into their hierarchical substructures has attracted much attention in recent decades.

Micro/nanofibrillated celluloses (M/NFCs) are usually prepared by intensive mechanical treatment, such as high-pressure homogenization (HPH), cryocrushing, grinding, and ultrasonication, which may or may not be preceded by enzymatic or chemical pretreatment. One of the major drawbacks of the intensive mechanical treatments required to achieve fibrillation of the cellulose walls is the high energy demand of the process. Various enzymatic and chemical pretreatments have been applied over the years to effectively reduce energy consumption and/or increase the degree of fibrillation [3].

One of the most popular chemical pretreatments, due to its proven effectiveness, is the oxidation of cellulose fibers by TEMPO-mediated oxidation. Electrostatic repulsion induced by the introduced negatively charged groups loosens the structure, causing the formation of individualized fibrils after a mild mechanical disintegration [4].

Depending on the combination of processes, different varieties of materials are obtained with very distinct morphological properties, surface chemistry, degree of polymerization, and degree of crystallinity. The final properties will dictate the different possible applications.

Among the different types of M/NFCs produced, unmodified or anionically modified materials are far more common than cationic cellulose products. Heinze et al. [5] reported the same tendency for the specific case of cellulose ethers. However, they also found that other cationic polysaccharide derivatives, such as cationic starch ethers, play

* Corresponding author.
E-mail address: jpedrosa@uc.pt (J.F.S. Pedrosa).

https://doi.org/10.1016/j.ijbiomac.2022.01.068
Received 1 October 2021; Received in revised form 7 December 2021; Accepted 11 January 2022
0141-8130/

a much greater role in commercial applications and are widely used in paper production (dry strength additive), textile and cosmetics industries.

The introduction of cationically charged groups, such as quaternary ammonium groups, into the cellulose structure can also be used as a pretreatment to improve fibrillation [6] and, at the same time, to expand the number of applications of M/NFCs. It is known that cationic materials have intrinsic antibacterial properties due to their affinity for negatively charged particles, such as the bacterial cell walls [7].

Because of these properties, cationic cellulose products have found their way into a variety of applications, being used as flocculants [8–10], adsorbents [11,12], stabilizers [13], and biocides [14,15], among others.

Although the cationization of cellulosic materials is not new [16–18], its use as a pretreatment for the preparation of M/NFC materials has only recently been published. To our knowledge, Aulin et al. [19] was the first author referencing it, using 2,3-epoxypropyltrimethylammonium chloride (EPTAC) as the cationizing agent followed by treatment in a high-pressure fluidizer. Since then, other cationic reagents have been tested for the preparation of cationic M/NFCs, such as chlorocholine chloride [6], Girard's reagent T (GT) [8, 15,20], aminoguanidine hydrochloride [21,22] or betaine hydrochloride [23].

A proper evaluation of the chemical and physical properties of fibrillated celluloses is of extreme importance in order to help tune their properties to the desired application. Since no single method was found to fully describe the properties and behavior of these materials, multiple methods must be combined for complete characterization [27]. Despite the recent growing interest in cationic M/NFCs, most of the published characterization results are generally limited to just a few techniques/parameters.

In this context, our work focuses on a more systematic characterization of cationic M/NFCs through the use of distinct complementary techniques. Special emphasis will be placed on the deconstruction effect suffered by cellulosic fibers. We also suggest for the first time the application of vacuum filtration to differentiate between yield of fibrillation due to dissolved material or stabilized fibrils. An alternative acid-base titration is also proposed for determining the degree of cationization. Laser diffraction, typically non applied for materials of high aspect ratio, is presented as a more expedite alternative to optical microscopy for the determination of the diameter distribution of cellulose fibers and fibrils.

A total of five cationic celluloses (one with CHPTAC and four with GT) with different degrees of cationicity were mechanically treated in a HPH to produce cationic M/NFCs. The morphological properties, chemical composition, and rheological behavior were evaluated to determine the effects of the degree of substitution (with GT) and the cationization method (for samples with a similar degree of substitution).

2. Materials and methods

2.1. Materials

Industrial unrefined and never dried BEKP, composed of 80–85 wt% cellulose, 14–19 wt% xylan, 0.3 wt% lignin and 0.4 wt% extractives [28], was used as the starting cellulose material.

The chemicals used in the cationization reactions were: sodium hydroxide pellets, acetic acid glacial ($C_2H_4O_2$, AA, from VWR), isopropanol (C_3H_8O, IPA, from Labsolve), (3-chloro-2-hydroxypropyl) trimethylammonium chloride ($C_6H_{15}Cl_2NO$, CHPTAC) 60 wt% aqueous solution, sodium periodate ($NaIO_4$, SP), and (carboxymethyl)trimethylammonium chloride hydrazide ($C_5H_{14}ClN_3O$, Girard's reagent T – GT, from Sigma-Aldrich). Hydroxylamine hydrochloride ($H_2NOH.HCl$), sodium hydroxide and hydrochloric acid 1 M aqueous solutions (all from Sigma-Aldrich) were used in the titrations for the determination of aldehyde groups and cationic charge. All chemicals were used as received without further purification. Distilled water was used throughout the work.

2.2. Preparation of cationic M/NFC

A direct and indirect method were used to covalently bond quaternary ammonium groups to bleached *Eucalyptus* kraft pulp (BEKP). For direct cationization, the most commonly used cationizing agent is EPTAC [24] or its precursor CHPTAC [25]. In this work, the reactive epoxide reagent was prepared in situ by reacting CHPTAC with alkali (Fig. 1 A). The epoxide was then reacted with the available hydroxyl groups of cellulose under alkaline conditions to form an ether linkage and produce the cationic cellulose.

In contrast, indirect cationization was carried out by a two-step cationization in which the cellulose was first converted into the more reactive form, dialdehyde cellulose (DAC), by oxidation with sodium metaperiodate (NaIO4). During oxidation, the two vicinal hydroxyl groups at the C2 and C3 positions of the anhydroglucose unit (AGU) are converted to aldehyde groups, with consequent cleavage of the C2-C3

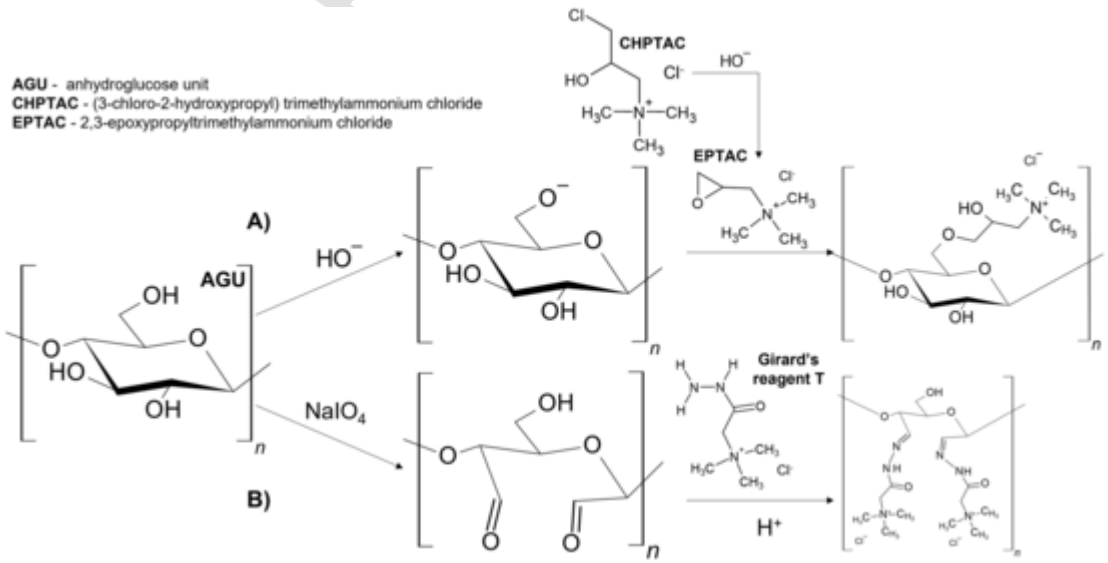

Fig. 1. Schematic representation of the cationic functionalization of cellulose with (A) CHPTAC and (B) Girard's reagent T.

bond [26]. The cationization was followed up by reacting the DAC with GT to form a stable imine structure possessing quaternary ammonium groups [8,9] (Fig. 1B).

For the cationization with CHPTAC, BEKP was dispersed in alkaline water at a consistency (C) of 3 wt% and a NaOH/AGU molar ratio of 9. The fiber suspension was left for 20 min at 20 °C, after which CHPTAC was added using a CHPTAC/AGU molar ratio of 6 [29,30]. The cationization was carried out at 65 °C for 8 h (Table 1). Subsequently, the cationized fibers were vacuum filtered through a filter paper with a pore size of 11 μm and washed several times with distilled water until the conductivity was constant.

Cationization with GT began with the preparation of DAC. For this, BEKP was dispersed in a water/IPA mixture (10%*v*/v IPA to act as a free radical scavenger and reduce the extent of depolymerization [31]), at 2.5 wt% and heated to 70 °C. To obtain different degrees of oxidation, a specific molar ratio of SP to AGU was added and the oxidation reaction was carried out for 4 h in the absence of light (to reduce photodegradation of SP). The parameters used for the oxidation reaction were adapted from the work of Sirvio et al. [32]. After oxidation, the obtained DACs were washed with water and the degree of substitution of the aldehyde groups (DSa) was determined by titration with sodium hydroxide according to the method described by Wei et al. [33], which is based on the oxime reaction between the aldehyde groups and hydroxylamine hydrochloride (Fig. S1) [32].

The undried DACs were dispersed in water acidified with 10%*v*/v of AA [34] at a consistency of 5 wt% and a specific molar ratio of GT to aldehyde groups was added. The cationization was performed at 70 °C for 1.5 h (Table 1). The cationic samples were vacuum filtered through a filter paper with a pore size of 11 μm and washed with a mixture of isopropanol/water (9:1 *v*/v) (to reduce the loss of solubilized cellulose) until the conductivity was constant.

The final micro/nanofibrillated cationic cellulose samples were produced by subjecting the cationized fibers to mechanical treatment in an HPH (GEA Niro Soavi, model Panther 115 NS3006L), with the first pass at 500 bar and a second pass at 700 bar. Homogenization was performed at room temperature with a pulp consistency of 1 wt%. The obtained cationic celluloses were labelled with the acronym CH or GT + (degree of substitution determined by elemental analysis). The resulting fibrillated samples were characterized as follows.

2.3. Characterization of cationic M/NFC

The nitrogen content (Nea, wt%) of the cationic celluloses was determined by elemental analysis (EA 1108 CHNS-O analyzer from Fisons) and used to determine the degree of cationic substitution (DSea, mol/mol), admitting all nitrogen detected comes from the grafted quaternary ammonium cations and the BEKP is composed exclusively by cellulose [30].

The charge density (CDt, mmol/g) was estimated using a potentiometric titration method [35]. In a typical titration, a given mass of cationic M/NFCs suspensions (corresponding to 200 mg dry) was dispersed in 150 mL of distilled water and the pH was adjusted to 11 with a 0.1 M aqueous NaOH solution, to convert the cationic quaternary ammonium groups to their OH^- form. The suspension was then titrated at 35 °C with 0.01 M HCl until the inflection point of the pH versus HCl volume curve was reached. The CDt value obtained was converted to the degree of substitution (DSt) and compared with the values obtained by elemental analysis. Further details on the calculations underlying the determinations of DS and CD can be found in the supplementary data (Section S2).

FTIR-ATR spectra were recorded on a Bruker Tensor 27 spectrometer with a MKII Golden Gate accessory, with 128 scans and a resolution of 4 cm^{-1}, in the range 650–4000 cm^{-1}. The spectra were treated for noise reduction, baseline slope and normalized.

X-ray diffraction (XRD) patterns of the samples were recorded with a Philips X'Pert diffractometer, operating in Bragg-Brentano geometry (θ-2θ), using CoKα radiation (λ = 1.78897 Å) and an applied voltage and current of 40 kV and 35 mA, respectively. Scans were performed at room temperature and collected over a range of 10°–40°, with a step of 0.025° and an acquisition time of 1 s per step. The crystallinity index (CI) was calculated from the peak intensity of the main crystalline plane (I_{002}) and from the minimum intensity between peaks 002 and 110 associated with the amorphous fraction of cellulose (I_{am}), according to the Segal formula (Eq. (1), Fig. 6) [36].

$$CI = \left(\left(I_{002} - I_{am}\right)/I_{002}\right) \times 100 \quad (1)$$

The yield of fibrillation was determined in duplicate after centrifugation of 40 ml of cationic cellulose aqueous suspension (0.2 wt%) at 9000 rpm for 30 min [37,38]. The weight percentage of the remaining material in the supernatant after centrifugation, determined by the difference between the original and centrifuged amounts, was considered as the "yield of fibrillation" (YF).

To determine the soluble fraction, a volume of 3 ml of the original cationic cellulose suspension was vacuum filtered through a cellulose acetate membrane filter (0.2 μm pore size). The filter was then dried (50 °C for 24 h) to quantify the mass retained and determine the percentage (wt%) of material on the filtrate. The material that was able to pass through the membrane was defined as 'soluble fraction 0.2' ($SF_{0.2}$). The results were obtained in duplicate.

Transmittance spectra of 0.1 wt% suspensions were recorded using a UV–Visible UVWin5 Software V5.0.5 spectrophotometer T60, at 600 nm and a medium speed scan of 2 $nm{\cdot}s^{-1}$. The transmittance was measured immediately after stirring the suspensions (0 h) and after 24 h without further stirring [38]. The spectrum of a cuvette filled with distilled water was used as a blank.

The average hydrodynamic diameter (*Z*-average) and the respective polydispersity index (PDI) of the soluble fraction of samples GT0.16 and GT0.36 (samples with the highest soluble fraction) were determined by dynamic light scattering (DLS) [38]. Measurements were performed in a Zetasizer NanoZS equipment (Malvern Instruments), with a 532 nm laser, using a backscatter angle detection of 173°. The samples were diluted to 0.1 wt%, carefully transferred to a glass cuvette and checked for the presence of bubbles.

To estimate the surface charge, zeta potential (ZP) was determined by electrophoretic light scattering (ELS) using the same equipment [38]. Measurements were performed on a diluted suspension (0.1 wt%) of the original BEKP and cationic cellulose samples.

All the results represent the average of three measurements performed under the following conditions: water as the dispersant, cellulose refractive index 1.47, dispersant refractive index 1.33, viscosity

Table 1
Reaction conditions used for the cationization of BEKP with CHPTAC and GT.

CHPTAC method								
Sample	Cellulose activation				Cellulose cationization			
	C (wt%)	NaOH/AGU (mol/mol)	T (°C)	t (h)	CHPTAC/AGU (mol/mol)	T (°C)	t (h)	
CH0.13	3	9	20	0.3	6	65	8	

GT method											
Sample	Cellulose oxidation						Cellulose cationization				
	C (wt%)	IPA (% v/v)	T (°C)	t (h)	SP/AGU (mol/mol)	DSa	C (wt%)	AA (% v/v)	GT/aldehyde (mol/mol)	T (°C)	t (h)
GT0.02	2.5	10	70	4	0.10	0.11	5	10	1	70	1.5
GT0.04					0.20	0.19			1		
GT0.16					0.55	0.48			0.7		
GT0.36					0.65	0.85			0.6		

0.8872 cP, temperature 25 °C. The data was analyzed according to the general calculation model for irregular particles.

The size of the original BEKP fibers and the cationic cellulose samples was also assessed by laser diffraction spectrometry (LDS) in a Mastersizer 2000 device (Malvern Instruments), equipped with a Hydro 2000MU module [38].

Prior to the measurements, a 0.2 wt% aqueous suspension of each sample was prepared and left under magnetic stirring (700 rpm) for 30 min. A certain volume of the prepared suspensions was added to 800 ml of water in the equipment vessel until an obscuration level of about 5% was reached, and the measurements were performed at a pump speed of 2000 rpm. The test was continued until the size stabilized. The final size distribution was set as the average of six consecutive measurements after size stabilization.

The scattering patterns were processed using the Mie theory model, assuming a refractive index and absorption of cellulose of 1.47 and 0.1, respectively.

By default, laser diffraction measurements produce volume-based particle size distributions. For comparison with the size measurements from microscopy analysis, the distributions were converted from volume-weighted to number-weighted distributions.

Polarized light optical microscopy (OM) images were acquired using an Olympus BH-2 KPA microscope (Olympus Optical Co., Ltd) equipped with a high-resolution CCD color camera (Olympus ColorView III).

A few drops of the cellulose suspensions were placed on a glass slide and allowed to dry at room temperature before analysis. Images were acquired at various magnifications using the analySIS software (Soft Imaging System GmbH).

The diameter of the observed fibers and fibrillar particles (measured at the center of the object) was determined using the ImageJ 1.53 g software [39]. Between 200 and 400 measurements were made for each sample. A distribution with the same mean and three standard deviations was fitted to the collected data. The obtained distributions were normalized and plotted on a logarithmic scale for comparison with the number distributions obtained by LDS.

The glass slide used for optical microscopy analysis was sputter coated with gold and field emission scanning electron microscopy (FE-SEM) images were acquired in a Carl Zeiss Merlin microscope with a Gemini II column, in secondary electron mode. The acceleration voltage used was 1 kV and the working distance was 3.4 mm.

The intrinsic viscosity ([η]) of all samples was measured using a standard capillary viscometer in 0.5 M cupriethylenediamine at 25 ± 0.1 °C. The obtained intrinsic viscosities were converted to the average degree of polymerization – $avgDP_{iv}$ by applying the Mark-Houwink equation (Eq. (2)) with the parameters defined by Henriksson et al. [40], specifically K = 0.42 and a = 1 (for a DP < 950) or K = 2.28 and a = 0.76 (for a DP > 950).

$$[\eta] = k.DP^{a} \quad (2)$$

Considering the samples as 100% cellulose, the average molecular weight – $avgMw_{iv}$ was determined by multiplying the $avgDP_{iv}$ by the molecular weight of AGU (162 g/mol).

Size exclusion chromatography (SEC) combined with a refractive index detector was used to determine the weight average molecular weight (avgMw) of the soluble fraction of samples GT0.16 and GT0.36 (Table 2). The SEC measurements were performed at 40 °C in an Agilent 1260 Infinity II High-Temperature GPC System equipped with two PL aquagel-OH Mixed-H 8 μm (300 × 7.5 mm) columns and a PL aquagel-OH 8 μm (50 × 7.5 mm) guard column. Samples were prepared in 0.1 M $NaNO_3$ aqueous solution at an approximate concentration of 1 mg/ml and made optically clean by filtration through 0.22 μm Millipore filters. The eluent was a 0.1 M $NaNO_3$ aqueous solution with a flow rate of 0.8 ml/min. Pullulan standards were used for calibration.

Rheological tests were performed at 20 °C in a Haake model RS1 controlled stress rheometer, using a cylindrical bob and cup sensor (Z34 DIN Ti) with a gap of 7.2 mm, connected to a temperature control recirculation bath (Haake Phoenix II). Flow curves were obtained in controlled stress mode applying shear stresses ranging between 0.2 and 50.0 Pa.

A systematization of the work presented in this paper, including the properties evaluated and the techniques used, is shown in Fig. 2.

3. Results and discussion

3.1. Chemical composition

During the cationization reaction, quaternary ammonium groups can be incorporated into the cellulose fiber structure (Fig. 1 A and B). The cationization of the fibers was confirmed by FTIR (Fig. 3) and ZP (Table 2).

In short, ZP can be seen as a measure of the effective electric charge of a particle surface in a liquid medium. Comparing the ZP of the prepared cationic M/NFC with the original BEKP, it can be observed that for all the samples, the ZP shifted from negative (−23 mV) to positive (from +24 to +30 mV), indicating the effective incorporation of positive charges into the surface of the cellulose fibers.

The chemical structure of the five cationic M/NFC samples and the original BEKP was inspected by FTIR analysis. The spectra obtained are presented in Fig. 3. For sample CH0.13, the successful cationization was

Table 2
Characterization of the cationic M/NFC samples.

	Sample					
	BEKP	CH0.13	GT0.02	GT0.04	GT0.16	GT0.36
Nea (wt%)	–	1.02 ± 0.04	0.60 ± 0.06	0.99 ± 0.02	3.61 ± 0.12	7.03 ± 0.02
DSea (mol/mol)	–	0.13 ± 0.01	0.02 ± 0.01	0.04 ± 0.01	0.16 ± 0.01	0.36 ± 0.01
CDt (mmol/g)	–	0.78 ± 0.01	0.23 ± 0.04	0.32 ± 0.03	0.90 ± 0.02	1.68 ± 0.04
DSt (mol/mol)	–	0.14 ± 0.01	0.04 ± 0.01	0.05 ± 0.01	0.17 ± 0.01	0.35 ± 0.01
CI (%)	80	70	69	73	76	57
[η] (ml/g)	999	965	183	102	20	11
$avgDP_{iv}$	2991	2859	437	244	47	26
$avgMw_{iv} \times 10^{-3}$ (Da)	485	464	71	40	8	4
ZP (mV)	−23 ± 5	+26 ± 3	+24 ± 2	+29 ± 5	+27 ± 2	+30 ± 3
Z-Average (d.nm)[a]	–	–	–	–	147.1 ± 3.6	106.4 ± 15.1
PDI[a]	–	–	–	–	0.37 ± 0.04	0.29 ± 0.04
$avgMw \times 10^{-3}$ (Da)[a, b]	–	–	–	–	1.081 ± 3.5 0.526 ± 0.5	1.025 ± 43 0.543 ± 4.5

[a] Measured for the soluble fraction of the sample.
[b] Bimodal distribution (available as supplementary data – Fig. S11 and S12).

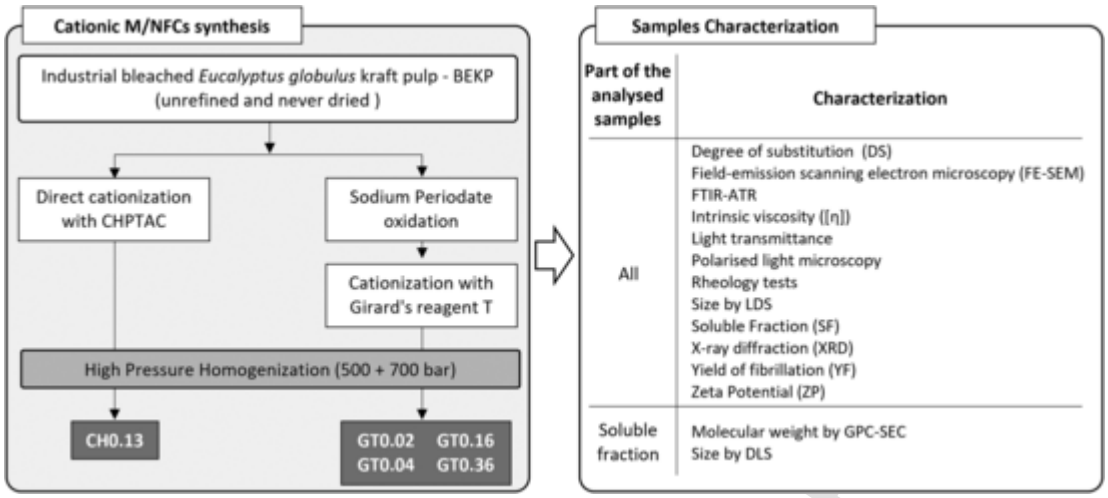

Fig. 2. Outline of the experimental work: cationic M/NFCs synthesis and samples characterization.

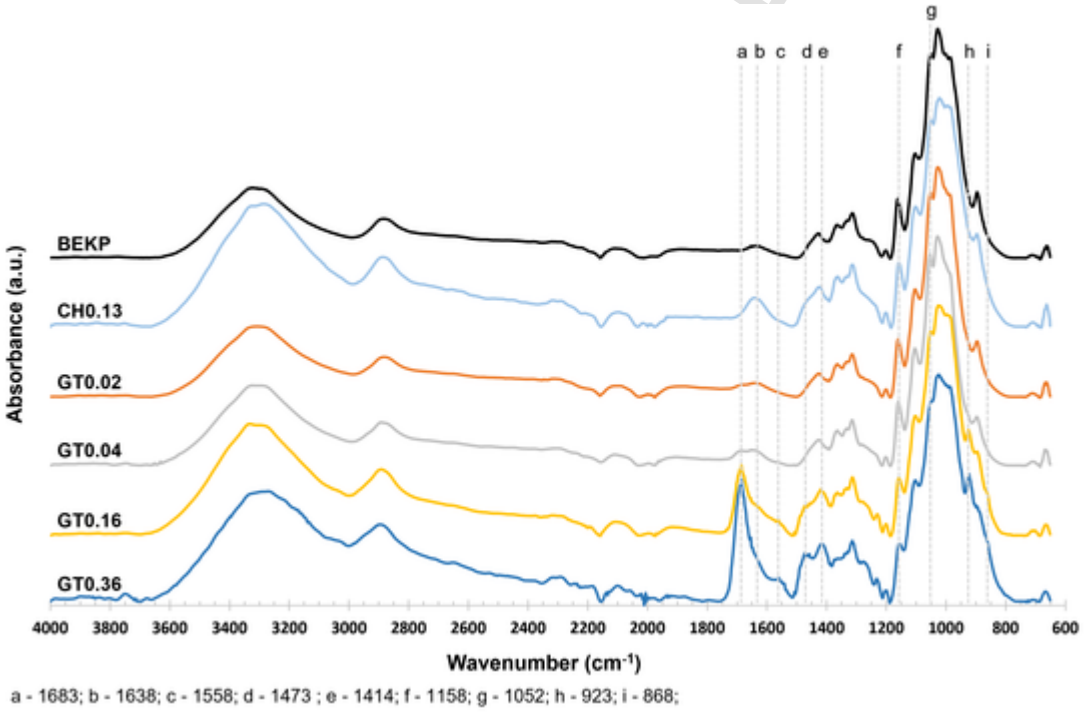

Fig. 3. FTIR-ATR spectra of the original BEKP and cationic M/NFC samples with different degrees of substitution.

evidenced by the appearance of a new peak at 1638 cm^{-1} (peak b) and a shoulder at 1473 cm^{-1} (peak d), which are related to the adsorption of water due to increased hydrophilicity [41] and to the stretching vibration of the methyl groups of the quaternary ammonium groups [42], respectively.

In the samples subjected to periodate oxidation and cationization with GT, a very clear peak appeared at 1683 cm^{-1} (peak a), which corresponds to the stretching of the carbonyl group on the hydrazide structure of GT [43]. The formation of an imine bond between the aldehyde groups of DAC and GT was confirmed by the peak at 1558 cm^{-1} (peak c) [43]. The bands at 1473 cm^{-1} and 1414 cm^{-1} (peaks d and e) were assigned to the asymmetric and symmetric bending of the methyl groups of GT, respectively [9]. The peak at 923 cm^{-1} (peak h) can be attributed to the asymmetric stretching of the C—N bond of quaternary ammonium [9], the N—N bond of GT [15,43] or even the stretching vibration of the C-C = bond of GT [44]. The decrease in intensity of the bands at 1158 cm^{-1} and 1052 cm^{-1} (peaks f and g) can be attributed to the weakened -OH absorbance resulting from the glucose ring-opening and oxidation of the OH groups at positions C2 and C3 to aldehyde groups [9,45]. The small peak at 868 cm^{-1} (peak i) can be attributed to the formation of hemiacetal bonds between residual aldehyde groups and adjacent hydroxyl groups [46].

The content of quaternary ammonium groups attached to the cellulose fibers was measured by elemental analysis and potentiometric titration (Table 2). Based on the amount of nitrogen quantified by elemental analysis, the obtained DS_{ea} were in the range of 0.02–0.36. The CDt of cationic groups on the cellulose surface was estimated by potentiometric titration and was in the range of 0.23–1.68 mmol/g. Conversion of the CDt results to DSt (0.04–0.35) gave similar results to those obtained by elemental analysis, suggesting that the titration method can be used as a rapid and cost-effective alternative to elemental analysis.

3.2. Morphological analysis

OM and FESEM analyses allow visualization of the structural changes undergone by the cellulose fibers when subjected to the different process steps (cationization and HPH treatment) (Fig. 4 and Figs. S6 to S10). Based on the OM images before HPH treatment and compared to the original BEKP, no evident changes were observed in samples CH0.13, GT0.02 and GT0.04. However, swelling of the fibers was observed in samples GT0.16 and GT0.36 as DS increased, with sample GT0.36 losing its fiber shape completely.

From a preliminary study of the impact of the degree of cationization on the depolymerization/solubilization of cationic celluloses obtained by the two-step method (data available as Supplementary data, Section S4), it was verified that under the conditions presented in this work (raw-material and reaction parameters), with a DS of 0.36, partially soluble cationic cellulose can be obtained. It was observed that for a DS in the range of 0.3–0.5, the fibers start to suffer morphological changes (swelling) (Fig. S11), presenting also between 20% and 40% of soluble material (Fig. S12). This range also coincides with the beginning of the level-off of the intrinsic viscosity curve, with values close to 30 ml/g (Fig. S13). At a DS ca.1, near 80% of the sample became soluble.

For example, Grenda et al. [47] obtained fully soluble cationic celluloses with a DS of 0.92~1.36 using also BEKP and performing the two-step cationization under similar experimental conditions.

After subjecting the cationized celluloses to HPH treatment, samples CH0.13 and GT0.16 became a transparent gel, with CH0.13 being thicker than GT0.16. The samples with lower DS (GT0.02 and GT0.04) remained a white fiber suspension, with a slight increase in viscosity. Finally, sample GT0.36 (highest DS) became a transparent and fluid suspension (slightly thicker than water).

Regarding the morphological changes of the fibers observed by OM, in sample CH0.13 some fibers remained intact, with long fibrils protruding from the main fiber body. In samples GT0.02 and GT0.04, most of the cellulose fibers broke into fragments of random sizes, with sample GT0.04 presenting smaller fragments. Some micro/nanofibrils are also seen, but these are shorter than those found in sample CH0.13. In samples GT0.16 and GT0.36, only residual small cellulose fiber fragments are found (the residual fragments found in sample GT0.16 were larger than in sample GT0.36), suggesting the solubilization of part of the material or a high degree of fibrillation (Table 2). The FESEM images of sample GT0.36 are consistent with those of OM, revealing several fragments of cellulose fibers and the absence of long fibrils, as observed in the other samples.

The level of deconstruction (fibrillation, dissolution, degradation) of the final materials was evaluated in terms of YF, $SF_{0.2}$, transmittance at 600 nm and [η] (Fig. 5).

As for the YF, the samples can be divided into two distinct groups. The first, with samples CH0.13, GT0.02 and GT0.04, and YF of 29%, 6% and 12%, respectively. The second, with GT0.16 and GT0.36 and a much higher YF (98% and 100%, respectively).

The method used to determine YF quantifies the amount of non-sedimentable material after centrifugation and does not distinguish between the fibrillated material that remains in suspension due to charge and steric stabilization (most important for materials with long fibrils, such as sample CH0.13) and/or the solubilized material. To differentiate between fibrils and soluble material, the samples were subjected to vacuum filtration through a membrane with a pore size of 0.2 μm. The material that was able to pass through the membrane was referred to as the soluble fraction – SF0.2.

For sample CH0.13, the $SF_{0.2}$ was zero, indicating that the YF obtained resulted exclusively from the stabilized fibrillated material. For all other samples, some soluble material was obtained. For samples GT0.02 and GT0.04, $SF_{0.2}$ was found to be 6% and 7%, respectively. These results are very similar to the YF obtained, suggesting that the soluble material present is responsible for the YF obtained.

Sample GT0.16 consists of 40% soluble material, which means that the YF of 98% results from a mixture of fibrillated and soluble material. Finally, for sample GT0.36, a YF and SF0.2 of 100% were obtained, indicating that the fibers were completely dissolved (except for the very small number of residual fiber fragments seen during microscopy analysis).

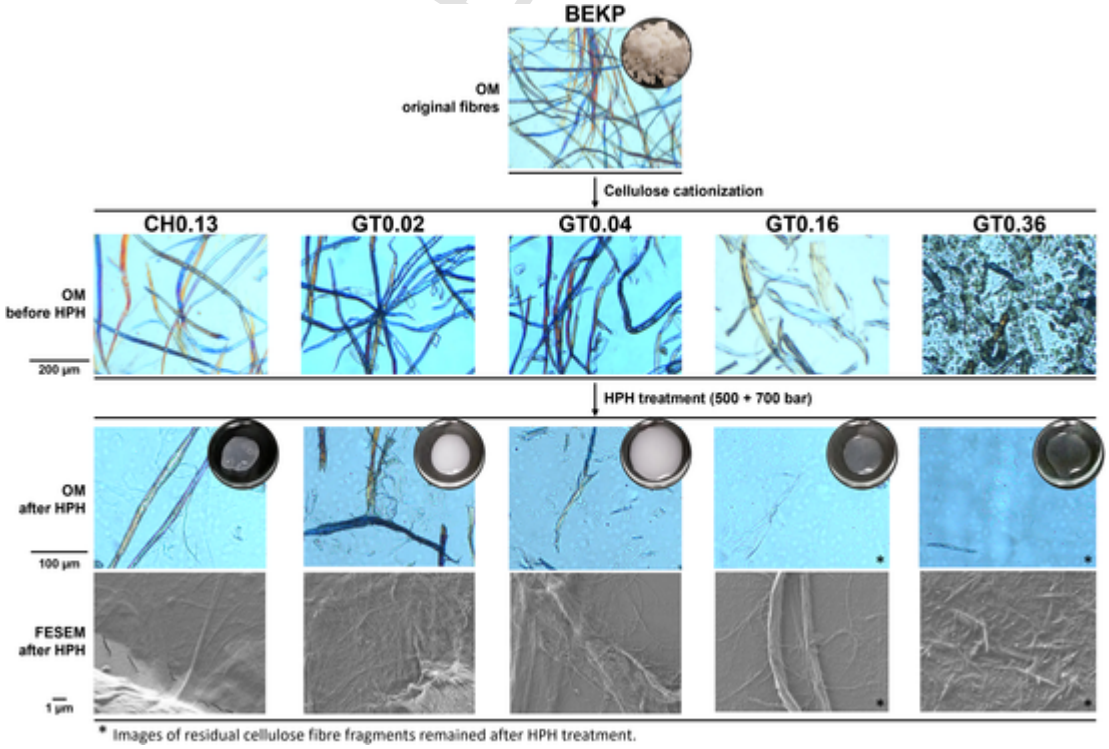

Fig. 4. Optical microscopy and FESEM images of the original BEKP and cationic cellulose samples before and after the mechanical treatment in the HPH.

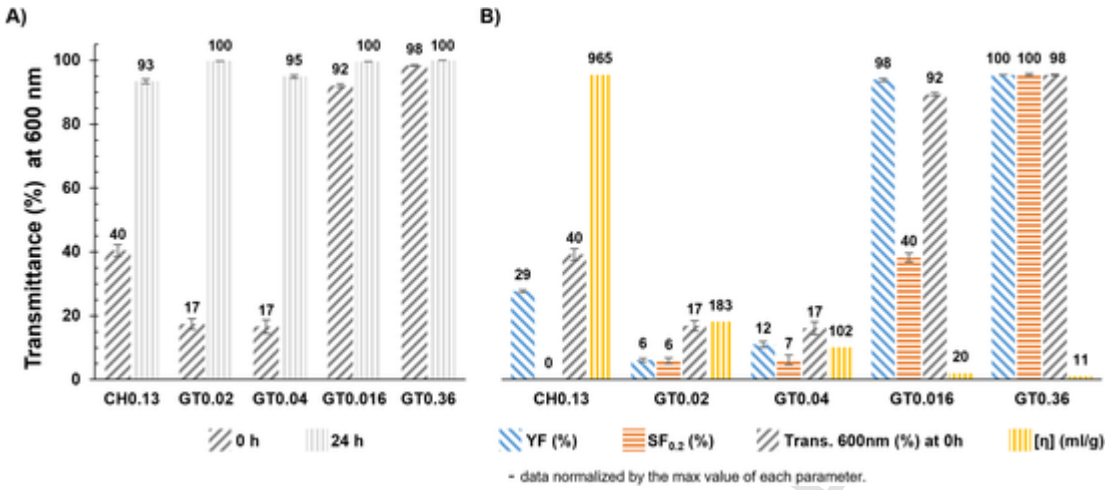

Fig. 5. A) Light transmittance at 600 nm of 0.1 wt% suspensions of the cationic M/NFC samples, measured at 0 and 24 h; B) Comparison between yield of fibrillation, soluble fraction, light transmittance at 0 h and intrinsic viscosity.

Samples CH0.13 and GT0.16, although having a similar DS, present very distinct YF (29% and 98%). Such results can be explained by the different amount of solubilized cellulose in each sample (0% and 40%, respectively).

The light transmittance of a material suspension (in this case cellulose fibers) can be used as an indication of the relative size of the suspended particles and extent of fibrillation [48]. The transmittance values of the sample suspensions measured at 0 h (Fig. 5) highly correlate with the obtained YF results, making it a good alternative method (faster and using less sample) for comparing the level of deconstruction of different samples. The transmittance values after 24 h were also recorded to determine the overall stability of the suspensions. Transmittance values increased for all samples, indicating the presence of sedimentable particles. A drastic increase was observed in samples CH0.13, GT0.02 and GT0.04 which increased from 40%, 17% and 17%, to 93%, 100% and 95%, respectively. The transmittance values of samples GT0.16 and GT0.36 increased to 100% due to sedimentation of the remaining fiber fragments. Sample CH0.13 had the lowest transmittance after 24 h (93%), which is due to the long fibrils (observed by microscopy) that can remain in suspension. The greatest change in transmittance was registered for sample GT0.02 (from 17% to 100%), due to the large fiber fragments with low DS that tend to sediment.

The intrinsic viscosity of a cellulose solution can be correlated with the degree of polymerization through the Mark-Houwink equation (Eq. (2)) and its values can give a clear indication of the level of degradation (DP reduction) of the polymeric cellulose chains. From the obtained viscosities (Table 2 and Fig. 5), a clear difference can be seen between the two cationization methods, with the two-step method leading to a lower intrinsic viscosity (higher degradation of the cellulose chains), that decreases with increasing DS. Negligible degradation was observed in sample CH0.13, with its intrinsic viscosity (965 mL/g) being only slightly lower than that of the original BEKP (999 mL/g). Such results were expected since periodate oxidation of cellulose leads to opening of the AGU ring with subsequent incorporation of aldehyde groups. It has been described that these electron-acceptor groups in the vicinity of the glycosidic oxygen can promote hydrolysis [49]. The acidic conditions during the cationization of DAC and the cavitation effect to which the weakened cellulose chains are subjected during the homogenization treatment may also be responsible for some of the demonstrated depolymerization. Solubilization of DAC in hot water, especially after functionalization, has also been reported in the literature [50,51] and justifies the increase of the soluble fraction of GT samples with increasing DS.

The crystalline structure of the cationic M/NFCs and the original BEKP was investigated by X-ray diffraction. Table 2 presents the CI calculated from the diffraction patterns presented in Fig. 6. All samples presented similar XRD patterns, with typical peaks of cellulose I, corresponding to the crystalline planes 1–10, 110 and 002 [29]. The lack of other peaks in the diffractograms of the cationic M/NFCs, suggests that no rearrangement of the cellulose I crystalline structure into other cellulose polymorphs occurred. The crystallinity of the original BEKP was ca. 80%, decreasing to 70, 69, 73, 76 and 57% for CH0.13, GT0.02, GT0.04, GT0.16 and GT0.36, respectively. The reduction in crystallinity indicates that the effects of the cationization and homogenization treatments were not limited to the surface of the fibers but also impacted the crystalline ordering of the cellulose.

Alkaline treatment of cellulose fibers, under certain conditions, is known to promote amorphization of the crystalline structure and conversion to cellulose II [30]. The alkaline conditions used during the cationization of the CH0.13 sample, although not strong enough to convert the crystalline structure from cellulose I to cellulose II, can justify the observed decrease in crystallinity. The reduction in crystallinity of the samples cationized by the two-step method can be attributed to the disruption of the structure due to the opening of the AGU rings, being the effect more evident for sample GT0.36, which suffered the most intense treatment.

Image-based techniques are very useful for evaluating the morphological changes that occur during the production of M/NFCs. However, this type of analysis is time consuming, operator dependent and limited to a very small fraction of the sample. For these reasons, LDS analysis was tested as a simple, faster and more representative alternative method for evaluating the size of fibrillar materials.

The number distributions of the diameters measured by OM for the original BEKP and cationic M/NFC samples were plotted using measurements from images at different magnifications (Fig. 7 A).

Samples CH0.13, GT0.02 and GT0.04 had the smallest sizes, with most fibrils having an average diameter of 1 μm. GT0.16 and GT0.36, although they were the most intensively treated, the average diameters (20 and 13 μm, respectively) were significantly higher than the other samples and similar to the original BEKP. These results can be explained by the high percentage of dissolved material found in samples GT0.16 and GT0.36, with only residual fragments (with diameters similar to the original BEKP) of the original fibers remaining in suspension.

The number-based particle size distributions obtained by LDS (converted from the volume-based distribution) for the original BEKP and cationic M/NFC samples are shown in Fig. 7 B. A quick comparison with the distributions obtained by microscopy analysis, allows us to verify that both sets of distributions agree with each other, including the relative positions of the peaks of the various samples. These results

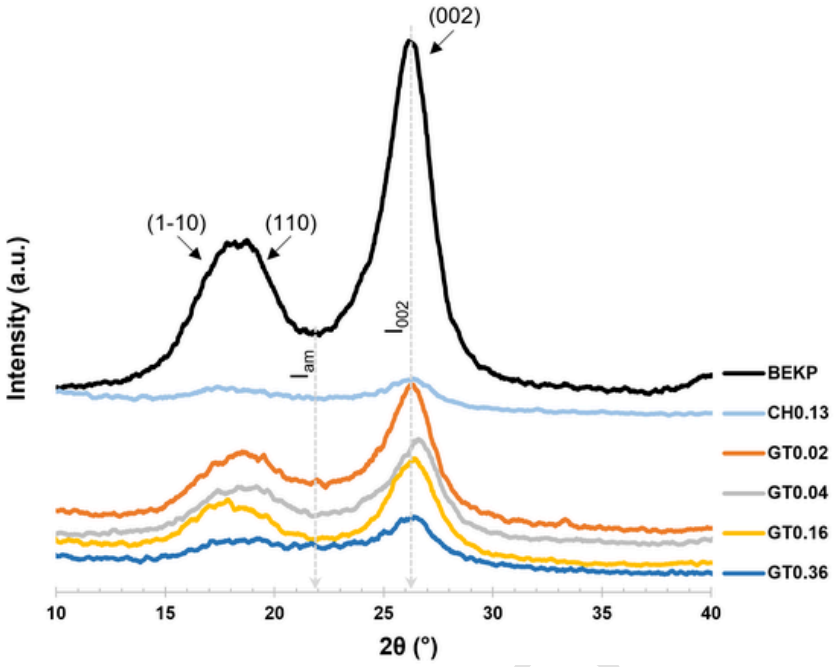

Fig. 6. XRD patterns of the original BEKP and cationic M/NFC samples.

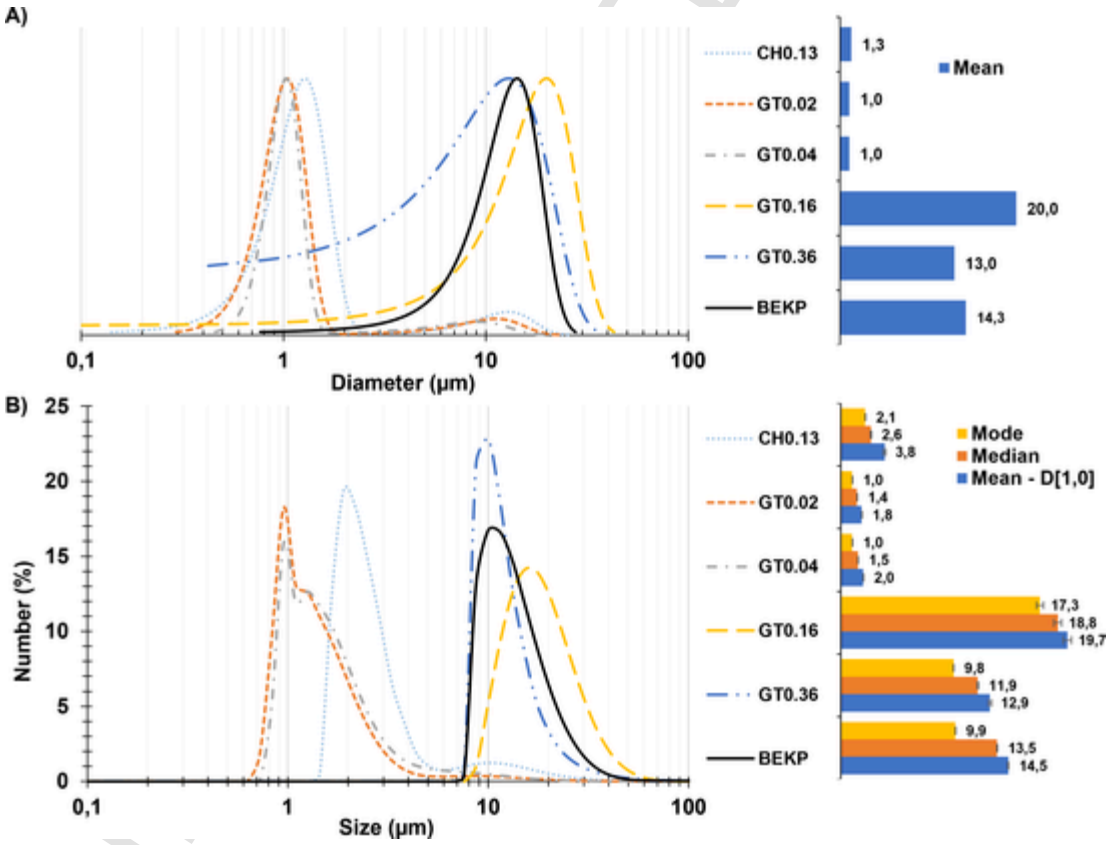

Fig. 7. A) Number distributions of diameters measured by optical microscopy for the original BEKP and cationic M/NFC samples. B) Number-based particle size distributions obtained by LDS for the original BEKP and cationic M/NFC samples.

suggest that LDS can be a useful technique for comparing the diameters of microfibrillar materials.

LDS provides an equivalent size-based distribution assuming that the light scattering pattern of the material is identical to that of spherical particles. For nonspherical particles, multimodal distributions can be obtained and the respective sizes can be attributed to the particle length and diameter [52]. For rod-shaped particles (such as cellulose fibrils), especially with high aspect ratio, the particles can align in the flow direction [53] and the peak associated with the fiber diameter becomes the most prevalent in the particle size distribution [52].

DLS and SEC analyses were used to determine the *Z*-average and avgMw of the soluble fraction of samples GT0.16 and GT0.36 (samples

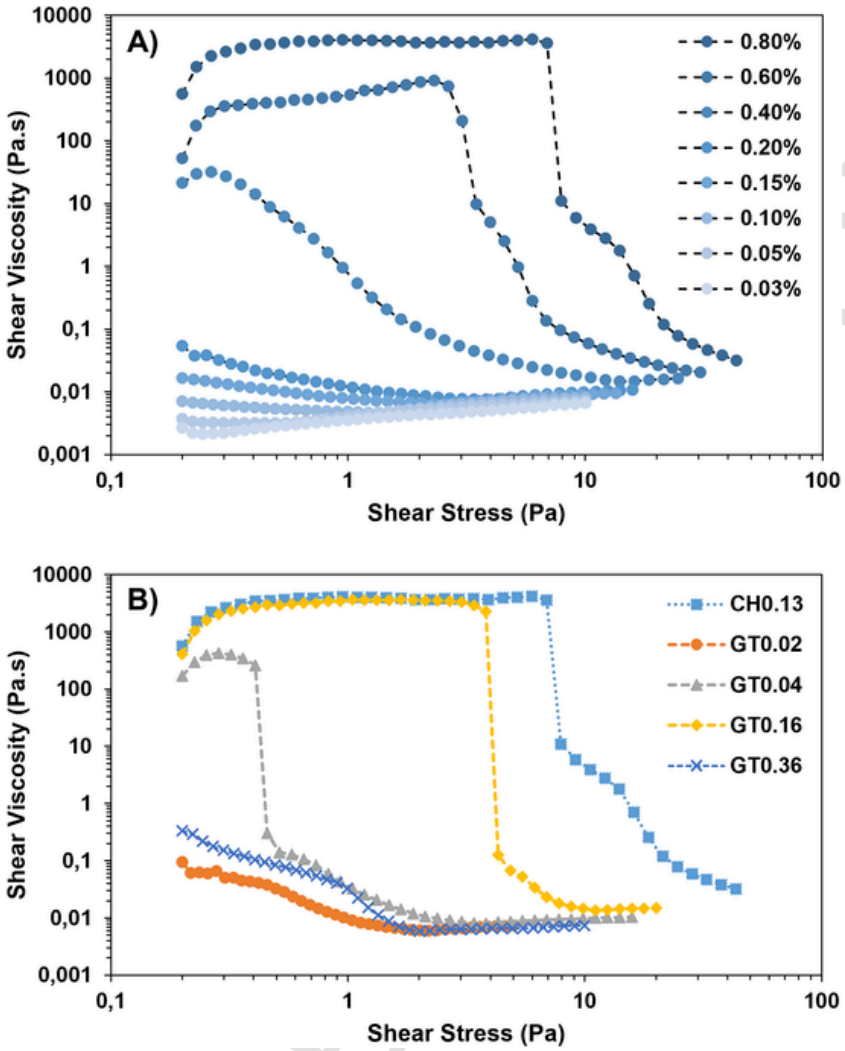

Fig. 8. A) Flow curves of CH0.13 aqueous suspensions as a function of shear stress, for different concentrations. B) Flow curves of 0.8 wt% aqueous suspensions of the obtained cationic M/NFC (different degrees of substitution) as a function of shear stress, All the experiments were performed at 25 °C.

with the highest soluble fraction) (Table 2). For both samples, a Z-average of 147 and 106 nm was determined with a corresponding PDI of the particle size distribution of 0.37 and 0.29, respectively. In terms of molecular weight, despite the difference in DS between samples GT0.16 and GT0.36, almost identical bimodal distributions were obtained (Figs. S14 and S15), with peaks around 1000 and 500 Da.

3.3. Rheology

The flow curves obtained for suspensions of cationic M/NFCs are shown in Fig. 8. As expected, the viscosity of the suspensions increased with increasing concentration (Fig. 8 A). Lower dilution suspensions presented a viscosity closer to water viscosity, and the suspensions with concentrations below 0.1 wt% behaved like Newtonian fluids. For the suspensions with intermediate concentrations, 0.15 and 0.20 wt%, it was observed a shear thinning behavior, as expected for polymeric solutions, due to the contact between the fibrils in suspension. At concentrations above 0.40%, a typical pseudoplastic curve was observed, with the appearance of a yield stress point, that was shifted at higher stresses with increasing M/NFC concentration. A similar behavior was observed for TEMPO oxidized cellulose nanofibers obtained from BEKP [54].

In addition to the M/NFC concentration, the cationization pretreatment also showed a great influence on the rheology of the suspensions. The fibers treated with CHPTAC resulted in suspensions with higher viscosity compared to those obtained from fibers treated with GT. This high viscosity is the result of a strong 3D fibril network, which is related to a good fibrillation of the material and also to the long and thin fibrils that can overlap, as as inferred from the microscopy and LDS results. However, the suspensions prepared from the pretreatment with GT showed a distinct behavior. At lower DS, the suspension exhibited very low viscosity, which is probably related to the low yield of fibrillation. The viscosity increased with increasing DS (up to sample GT0.16), indicating better fibrillation and thus the formation of an entangled network. However, at a higher DS the viscosity of the suspension decreases, which is a consequence of the extensive degradation of the cellulose fibers and consequently the absence or reduction of entanglements.

The volume occupied by a polymeric particle in a solution or suspension and the formation of the entangled network are closely related [55]. Longer fibrils have a higher equivalent volume and therefore above a specific concentration (overlap concentration - c*), they can more easily touch the neighboring fibrils and form a network. Polymers with high Mw can be expected to have lower c*. Similarly, longer fibrils (higher DP) also present lower c* compared to short fibrils (lower DP). As can be seen in Fig. 9, sample CH0.13 (with an estimated DP of 2859) had the lowest overlap concentration, ca. 0.13 wt%. Samples GT0.02, GT0.04 and GT0.16 presented c* values in the range of ca. 0.3–0.4 wt%, in agreement with the DP estimated by intrinsic viscosity (DP of 437, 244 and 47, respectively).

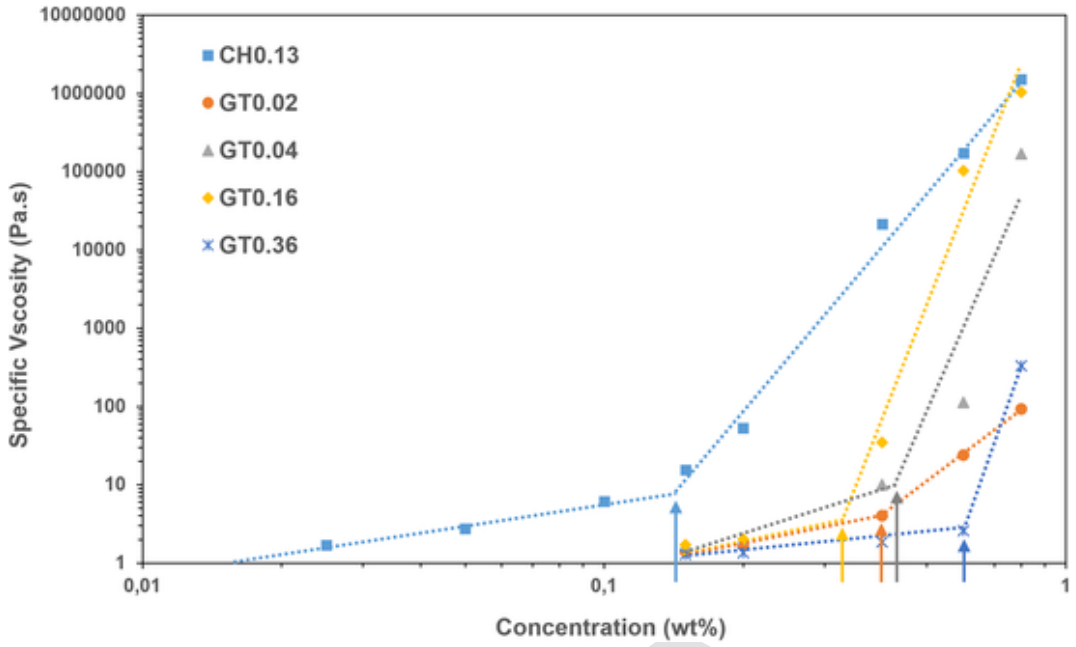

Fig. 9. Critical overlap concentration of the obtained cationic M/NFC.

A lower c* value was observed for sample GT0.16 compared to GT0.02 and GT0.04, despite the lower DP, being probably related with the higher yield of fibrillation, which means more fibrils in suspension for the same concentration. Sample GT0.36 presented the higher overlap concentration value, ca. 0.6 wt% due to the very low DP and almost complete solubilization of the cellulose fibers, which resulted in a low equivalent volume and made the interaction between the fibrils difficult.

4. Conclusions

A direct and a two-step cationization methods were evaluated as pretreatments for the preparation of cationic M/NFCs by high-pressure homogenization. The direct reaction of cellulose with EPTAC resulted in the formation of a transparent gel (at 1 wt%). This sample (CH0.13) had the lowest critical overlap concentration as a consequence of the long fibrils still attached to the main fiber body and diameters averaging 1 μm or less. No considerable degradation of the polymeric cellulose chains was observed.

On the other hand, the two-step method involving sodium periodate oxidation followed by reaction with Girard's reagent T caused significant degradation of the cellulose structure, with none of the samples becoming a firm gel, like sample CH0.13 (even with a similar DS, like sample GT0.16). Low DS (0.02 and 0.04) led to the formation of short fibrils and a small fraction of solubilized material (6 to 7%). The increase in DS promoted further solubilization of the cellulose fibers, resulting in 40% solubilized material for a DS of 0.16 and almost complete solubilization for a DS of 0.36.

CRediT authorship contribution statement

Jorge F. S. Pedrosa: Conceptualization, Investigation, Methodology, Writing - original draft, Writing - review & editing. Maria G. Rasteiro: Supervision, Writing - review & editing. Carlos P. Neto: Funding acquisition, Writing - review & editing. Paulo J. T. Ferreira: Supervision, Writing - review & editing, Funding acquisition, Project administration.

Declaration of competing interest

The authors declare that they have no known competing financial interests or personal relationships that could have appeared to influence the work reported in this paper.

Acknowledgements

This work was carried out under the Project inpactus – innovative products and technologies from eucalyptus, Project N.° 21874 funded by Portugal 2020 through European Regional Development Fund (ERDF) in the frame of COMPETE 2020 n°246/AXIS II/2017. The authors also want to acknowledge the Strategic Research Centre Project UIDB/00102/2020, funded by the Fundação para a Ciência e Tecnologia (FCT), Project ToxApp4NanoCELFI (PTDC/SAU-PUB/32587/2017, from the Foundation for Science and Technology, Portugal), and the Network CYTED Nanocelia - Transferencia Tecnológica sobre Aplicaciones de Nanocelulosa en Iberoamérica.

Appendix A. Supplementary data

Supplementary data to this article can be found online at https://doi.org/10.1016/j.ijbiomac.2022.01.068.

References

[1] D. Trache, M.H. Hussin, C.T.H. Chuin, S. Sabar, M.R.N. Fazita, O.F.A. Taiwo, T.M. Hassan, M.K.M. Haafiz, Microcrystalline cellulose: isolation, characterization and bio-composites application—a review, Int. J. Biol. Macromol. 93 (2016) 789–804, https://doi.org/10.1016/j.ijbiomac.2016.09.056.
[2] L. Alves, B. Medronho, A. Filipe, A. Romano, M.G. Rasteiro, B. Lindman, D. Topgaard, I. Davidovich, Y. Talmon, Revisiting the dissolution of cellulose in H3PO4(aq) through cryo-TEM, PTssNMR and DWS, Carbohydrate Polymers 252 (2021) 117122, https://doi.org/10.1016/j.carbpol.2020.117122.
[3] O. Nechyporchuk, M.N. Belgacem, J. Bras, Production of cellulose nanofibrils: a review of recent advances, Ind. Crop. Prod. 93 (2016) 2–25, https://doi.org/10.1016/j.indcrop.2016.02.016.
[4] A. Isogai, T. Saito, H. Fukuzumi, TEMPO-oxidized cellulose nanofibers, Nanoscale 3 (2011) 71–85, https://doi.org/10.1039/c0nr00583e.
[5] T. Heinze, O.A.E. Seoud, A. Koschella, Cellulose Derivatives: Synthesis, Structure, and Properties, Springer International Publishing, 2018.
[6] T.T.T. Ho, T. Zimmermann, R. Hauert, W. Caseri, Preparation and characterization of cationic nanofibrillated cellulose from etherification and high-shear disintegration processes, Cellulose 18 (2011) 1391–1406, https://doi.org/10.1007/s10570-011-9591-2.

[7] M. Tavakolian, S.M. Jafari, T.G.M. van de Ven, A review on surface-functionalized cellulosic nanostructures as biocompatible antibacterial materials, Nano-Micro Lett. 12 (2020) 73, https://doi.org/10.1007/s40820-020-0408-4.

[8] H. Liimatainen, T. Suopajärvi, J. Sirviö, O. Hormi, J. Niinimäki, Fabrication of cationic cellulosic nanofibrils through aqueous quaternization pretreatment and their use in colloid aggregation, Carbohydr. Polym. 103 (2014) 187–192, https://doi.org/10.1016/j.carbpol.2013.12.042.

[9] K. Grenda, J. Arnold, J.A.F. Gamelas, M.G. Rasteiro, Environmentally friendly cellulose-based polyelectrolytes in wastewater treatment, Water Sci. Technol. 76 (2017) 1490–1499, https://doi.org/10.2166/wst.2017.299.

[10] Z. Lu, X. An, H. Zhang, L. Liu, H. Dai, H. Cao, B. Lu, H. Liu, Cationic cellulose nano-fibers (CCNF) as versatile flocculants of wood pulp for high wet web performance, Carbohydr. Polym. 229 (2020) 115434, https://doi.org/10.1016/j.carbpol.2019.115434.

[11] W. Maatar, S. Boufi, Microporous cationic nanofibrillar cellulose aerogel as promising adsorbent of acid dyes, Cellulose 24 (2017) 1001–1015, https://doi.org/10.1007/s10570-016-1162-0.

[12] A. Mautner, T. Kobkeatthawin, A. Bismarck, Efficient continuous removal of nitrates from water with cationic cellulose nanopaper membranes, in: Resource-Efficient Technologies, 3, 2017, pp. 22–28, https://doi.org/10.1016/j.reffit.2017.01.005.

[13] C.E.P. Silva, K.C. Tam, J.S. Bernardes, W. Loh, Double stabilization mechanism of O/W Pickering emulsions using cationic nanofibrillated cellulose, J. Colloid Interface Sci. (2020), https://doi.org/10.1016/j.jcis.2020.04.001.

[14] S. Saini, Ç. Yücel Falco, M.N. Belgacem, J. Bras, Surface cationized cellulose nanofibrils for the production of contact active antimicrobial surfaces, Carbohydr. Polym. 135 (2016) 239–247, https://doi.org/10.1016/j.carbpol.2015.09.002.

[15] C.G. Otoni, J.S.L. Figueiredo, L.B. Capeletti, M.B. Cardoso, J.S. Bernardes, W. Loh, Tailoring the antimicrobial response of cationic nanocellulose-based foams through cryo-templating, ACS Appl. Bio Mater. 2 (2019) 1975–1986, https://doi.org/10.1021/acsabm.9b00034.

[16] M. Antal, A. Ebringerová, I. Šimkovic, New aspects in cationization of lignocellulose materials. I. Preparation of lignocellulose materials containing quarternary ammonium groups, J. Appl. Polym. Sci. 29 (1984) 637–642, https://doi.org/10.1002/app.1984.070290219.

[17] W.R. Goynes, R.R. Benerito, Effects of associated anion on hydrophilicity of quaternary ammonium cellulose, J. Appl. Polym. Sci. 36 (1988) 1255–1281, https://doi.org/10.1002/app.1988.070360603.

[18] M. Pašteka, Quaternization of regenerated cellulose under homogeneous reaction conditions, Acta Polymerica. 39 (1988) 130–132, https://doi.org/10.1002/actp.1988.010390309.

[19] C. Aulin, E. Johansson, L. Wågberg, T. Lindström, Self-organized films from cellulose I nanofibrils using the layer-by-layer technique, Biomacromolecules 11 (2010) 872–882, https://doi.org/10.1021/bm100075e.

[20] S.D. Hujaya, G.S. Lorite, S.J. Vainio, H. Liimatainen, Polyion complex hydrogels from chemically modified cellulose nanofibrils: structure-function relationship and potential for controlled and pH-responsive release of doxorubicin, Acta Biomater. 75 (2018) 346–357, https://doi.org/10.1016/j.actbio.2018.06.013.

[21] T. Suopajärvi, J.A. Sirviö, H. Liimatainen, Cationic nanocelluloses in dewatering of municipal activated sludge, journal of environmental, Chem. Eng. 5 (2017) 86–92, https://doi.org/10.1016/j.jece.2016.11.021.

[22] P. Li, J.A. Sirviö, A. Haapala, A. Khakalo, H. Liimatainen, Anti-oxidative and UV-absorbing biohybrid film of cellulose nanofibrils and tannin extract, Food Hydrocoll. 92 (2019) 208–217, https://doi.org/10.1016/j.foodhyd.2019.02.002.

[23] J.A. Sirviö, Cationization of lignocellulosic fibers with betaine in deep eutectic solvent: facile route to charge stabilized cellulose and wood nanofibers, Carbohydr. Polym. 198 (2018) 34–40, https://doi.org/10.1016/j.carbpol.2018.06.051.

[24] M. Hasani, E.D. Cranston, G. Westman, D.G. Gray, Cationic surface functionalization of cellulose nanocrystals, Soft Matter 4 (2008) 2238–2244, https://doi.org/10.1039/B806789A.

[25] Y. Song, Y. Sun, X. Zhang, J. Zhou, L. Zhang, Homogeneous quaternization of cellulose in NaOH/Urea aqueous solutions as gene carriers, Biomacromolecules 9 (2008) 2259–2264, https://doi.org/10.1021/bm800429a.

[26] T. Nikolic, M. Kostic, J. Praskalo, Z. Petronijevic, P. Skundric, Sorption properties of periodate oxidized cotton, Chem. Ind. Chem. Eng. Q. 17 (2011) 367–374, https://doi.org/10.2298/CICEQ110521023N.

[27] H. Kangas, P. Lahtinen, A. Sneck, A.-M. Saariaho, O. Laitinen, E. Hellén, Characterization of fibrillated celluloses. A short review and evaluation of characteristics with a combination of methods 29 (2014) 129–143, https://doi.org/10.3183/NPPRJ-2014-29-01-p129-143.

[28] P. Henriques, M. Martinho, M.d.L. Serrano, A.P. Mende. de Sousa, A.M. Brite. Alves, Xylooligosaccharides production by acid hydrolysis of an alkaline extraction filtrate from Eucalyptus globulus bleached kraft pulp 159 (2021) 113066, https://doi.org/10.1016/j.indcrop.2020.113066.

[29] R. Aguado, A.F. Lourenço, P.J. Ferreira, A. Moral, A. Tijero, Cationic cellulosic derivatives as flocculants in papermaking, Cellulose 24 (2017) 3015–3027, https://doi.org/10.1007/s10570-017-1313-y.

[30] R. Aguado, A.F. Lourenço, P.J.T. Ferreira, A. Moral, A. Tijero, The relevance of the pretreatment on the chemical modification of cellulosic fibers, Cellulose 26 (2019) 5925–5936, https://doi.org/10.1007/s10570-019-02517-7.

[31] K.A. Kristiansen, A. Potthast, B.E. Christensen, Periodate oxidation of polysaccharides for modification of chemical and physical properties, Carbohydr. Res. 345 (2010) 1264–1271, https://doi.org/10.1016/j.carres.2010.02.011.

[32] J. Sirvio, U. Hyvakko, H. Liimatainen, J. Niinimaki, O. Hormi, Periodate oxidation of cellulose at elevated temperatures using metal salts as cellulose activators, Carbohydr. Polym. 83 (2011) 1293–1297, https://doi.org/10.1016/j.carbpol.2010.09.036.

[33] J. Wei, C. Du, H. Liu, Y. Chen, H. Yu, Z. Zhou, Preparation and characterization of aldehyde-functionalized cellulosic fibers through periodate oxidization of bamboo pulp, Bioresources 11 (2016) 8386–8395, https://doi.org/10.15376/biores.11.4.8386-8395.

[34] H. Hong, Y. Wang, Derivatization with Girard reagent T combined with LC–MS/MS for the sensitive detection of 5-Formyl-2'-deoxyuridine in cellular DNA, Anal. Chem. 79 (2007) 322–326, https://doi.org/10.1021/ac061465w.

[35] A.A. Shunkevich, Z.I. Akulich, G.V. Mediak, V.S. Soldatov, Acid–base properties of ion exchangers. III. Anion exchangers on the basis of polyacrylonitrile fiber, React. Funct. Polym. 63 (2005) 27–34, https://doi.org/10.1016/j.reactfunctpolym.2005.02.002.

[36] L. Segal, J.J. Creely, A.E. Martin, C.M. Conrad, An empirical method for estimating the degree of crystallinity of native cellulose using the X-ray diffractometer, Text. Res. J. 29 (1959) 786–794, https://doi.org/10.1177/004051755902901003.

[37] S. Alila, I. Besbes, M.R. Vilar, P. Mutjé, S. Boufi, Non-woody plants as raw materials for production of microfibrillated cellulose (MFC): a comparative study, Ind. Crop. Prod. 41 (2013) 250–259, https://doi.org/10.1016/j.indcrop.2012.04.028.

[38] J.A.F. Gamelas, J. Pedrosa, A.F. Lourenço, P. Mutjé, I. González, G. Chinga-Carrasco, G. Singh, P.J.T. Ferreira, On the morphology of cellulose nanofibrils obtained by TEMPO-mediated oxidation and mechanical treatment, Micron 72 (2015) 28–33, https://doi.org/10.1016/j.micron.2015.02.003.

[39] C.A. Schneider, W.S. Rasband, K.W. Eliceiri, NIH image to ImageJ: 25 years of image analysis, Nat. Methods 9 (2012) 671–675, https://doi.org/10.1038/nmeth.2089.

[40] M. Henriksson, L.A. Berglund, P. Isaksson, T. Lindström, T. Nishino, Cellulose nanopaper structures of high toughness, Biomacromolecules 9 (2008) 1579–1585, https://doi.org/10.1021/bm800038n.

[41] N. Odabas, H. Amer, M. Bacher, U. Henniges, A. Potthast, T. Rosenau, Properties of cellulosic material after cationization in different solvents, ACS Sustain. Chem. Eng. 4 (2016) 2295–2301, https://doi.org/10.1021/acssuschemeng.5b01752.

[42] Y. Song, J. Zhang, W. Gan, J. Zhou, L. Zhang, Flocculation properties and antimicrobial activities of quaternized celluloses synthesized in NaOH/urea aqueous solution, Ind. Eng. Chem. Res. 49 (2010) 1242–1246, https://doi.org/10.1021/ie9015057.

[43] X. Huang, G. Dognani, P. Hadi, M. Yang, A.E. Job, B.S. Hsiao, Cationic dialdehyde nanocellulose from sugarcane bagasse for efficient Chromium(VI) removal, ACS Sustain. Chem. Eng. 8 (2020) 4734–4744, https://doi.org/10.1021/acssuschemeng.9b06683.

[44] Y. Liu, Y. Yu, Q. Wang, J. Xu, X. Fan, P. Wang, J. Yuan, Biological–chemical modification of cellulose nanocrystal to prepare highly compatible chitosan-based nanocomposites, Cellulose 26 (2019) 5267–5279, https://doi.org/10.1007/s10570-019-02486-x.

[45] L. Zhang, P. Yan, Y. Li, X. He, Y. Dai, Z. Tan, Preparation and antibacterial activity of a cellulose-based Schiff base derived from dialdehyde cellulose and L-lysine, Ind. Crop. Prod. 145 (2020) 112126, https://doi.org/10.1016/j.indcrop.2020.112126.

[46] P. Calvini, A. Gorassini, G. Luciano, E. Franceschi, FTIR and WAXS analysis of periodate oxycellulose: evidence for a cluster mechanism of oxidation, Vib. Spectrosc. 40 (2006) 177–183, https://doi.org/10.1016/j.vibspec.2005.08.004.

[47] K. Grenda, J. Arnold, J.A.F. Gamelas, O.J. Cayre, M.G. Rasteiro, Flocculation of silica nanoparticles by natural, wood-based polyelectrolytes, Sep. Purif. Technol. 231 (2020) 115888, https://doi.org/10.1016/j.seppur.2019.115888.

[48] I. Besbes, M.R. Vilar, S. Boufi, Nanofibrillated cellulose from alfa, eucalyptus and pine fibres: preparation, characteristics and reinforcing potential, Carbohydr. Polym. 86 (2011) 1198–1206, https://doi.org/10.1016/j.carbpol.2011.06.015.

[49] F. Coppola, A. Modelli, Oxidative degradation of non-recycled and recycled paper, Cellulose 27 (2020) 8977–8987, https://doi.org/10.1007/s10570-020-03395-0.

[50] U.-J. Kim, M. Wada, S. Kuga, Solubilization of dialdehyde cellulose by hot water, Carbohydr. Polym. 56 (2004) 7–10, https://doi.org/10.1016/j.carbpol.2003.10.013.

[51] C.-W. Yang, H.-M. Choi, Preparation of water-soluble dialdehyde nanocelluloses by periodate oxidation under microwave irradiation, Cellul. Chem. Technol. 54 (2020) 247–258, https://doi.org/10.35812/CelluloseChemTechnol.2020.54.26.

[52] D.M. Scott, Interpreting Laser Diffraction Results for Non-Spherical Particles, 2019. https://static.horiba.com/fileadmin/Horiba/Products/Scientific/Particle_Characterization/Webinars/Interpreting_Diffraction_Results_for_Non-Spherical_Particles.pdf. (Accessed 29 July 2021).

[53] C. Berthold, R. Klein, J. Lühmann, K.G. Nickel, Characterization of fibres and fibre collectives with common laser diffractometers 17 (2000) 113–116, https://doi.org/10.1002/1521-4117(200010)17:3<113::AID-PPSC113>3.0.CO;2-Z.

[54] L. Alves, E. Ferraz, A.F. Lourenço, P.J. Ferreira, M.G. Rasteiro, J.A.F. Gamelas, Tuning rheology and aggregation behaviour of TEMPO-oxidised cellulose nanofibrils aqueous suspensions by addition of different acids, Carbohydr. Polym. 237 (2020) 116109, https://doi.org/10.1016/j.carbpol.2020.116109.

[55] L. Alves, B. Lindman, B. Klotz, A. Böttcher, H.-M. Haake, F.E. Antunes, Rheology of polyacrylate systems depends strongly on architecture, Colloid Polym. Sci. 293 (2015) 3285–3293, https://doi.org/10.1007/s00396-015-3715-4.